ISSN 1063-7761, Journal of Experimental and Theoretical Physics, 2014, Vol. 119, No. 6, pp. 1102–1108. © Pleiades Publishing, Inc., 2014.

Optical and Mechanical Properties of Electron Bubbles in Superfluid Helium-4[1]

Z. Xie, W. Wei, Y. Yang, and H. J. Maris*

Department of Physics, Brown University, Providence, Rhode Island, 02912 USA

**e-mail: humphrey_maris@brown.edu*

Received May 14, 2014

Abstract—A series of experiments has revealed the existence of a large number (about 18) of different types of negative ions in superfluid helium-4. Despite much effort, the physical nature of these "exotic ions" has still not been determined. We discuss possible experiments which may be able to help determine the structure of these objects.

Contribution for the JETP special issue in honor of A.F. Andreev's 75th birthday

DOI: 10.1134/S1063776114120103

1. INTRODUCTION

At first sight, it appears that it should be easy to understand the behavior of an electron immersed in liquid helium. Because a helium atom has a closed shell of electrons, there is a strong repulsion between a helium atom and an electron. As a result, in order to enter liquid helium, an electron has to overcome an energy barrier of approximately 1 eV [1a]. An experiment performed earlier [1b] gave the result 1.3 eV. This barrier, together with the very low surface energy α of the liquid (0.375 erg cm^{-2}) [2], makes it favorable for an electron to force open a cavity in the liquid and become trapped there, rather than moving freely through the bulk liquid. The size of this bubble can be estimated, to a reasonable accuracy, from the approximate expression for the energy

$$E_{\text{bubble}} = \frac{h^2}{8mR^2} + 4\pi R^2\alpha + \frac{4\pi}{3}R^3P, \qquad (1)$$

where R is the bubble radius, m is the electron mass, and the last term represents the energy associated with forming the bubble when a pressure P is applied to the liquid. In the absence of an applied pressure, we find from Eq. (1) that the energy should be a minimum for the radius

$$R_0 = \left(\frac{h^2}{32\pi m\alpha}\right)^{1/4} \approx 19\ \text{Å}. \qquad (2)$$

These "electron bubbles" have been studied in many experiments.

1—Measurements have been made of the photon energies required to excite the electron to a higher energy state [3–5]. Since these energies are dependent on the bubble size (approximately proportional to the inverse square of the radius), the experiments provide information about the radius.

2—The mechanical properties of the bubble can be studied by applying a negative pressure [6]. If a negative pressure larger than a critical value P_c is applied, the bubble becomes unstable and grows rapidly. It can then be detected optically. From Eq. (1), the critical pressure is found to be [7]

$$P_c = -\frac{16}{5}\left(\frac{2\pi m}{5h^2}\right)^{1/4}\alpha^{5/4}. \qquad (3)$$

3—Measurements have been made of the mobility μ of these bubbles [8–10]. The mobility is limited by the drag force exerted on a moving bubble by thermally excited phonons and rotons. In superfluid helium-4 above 1 K, the drag is primarily due to rotons and the mobility can be expected to vary as

$$\mu \propto \exp(\Delta/kT), \qquad (4)$$

where Δ is the roton energy gap. The results of the mobility experiments give a temperature dependence in reasonable agreement with this. If a sufficiently large electric field is applied, the velocity reaches a critical value v_c at which a quantized vortex ring is nucleated. The bubble then becomes attached to this vortex ring [11].

4—The effective mass of the bubbles has been measured under the saturated vapor pressure [12] and under elevated pressure [13]. The results of the measurements are in good agreement with the values predicted from the bubble model.

Surprisingly, the experiments have revealed that in addition to the "normal" electron bubbles (NEB),

[1] The article is published in the original.

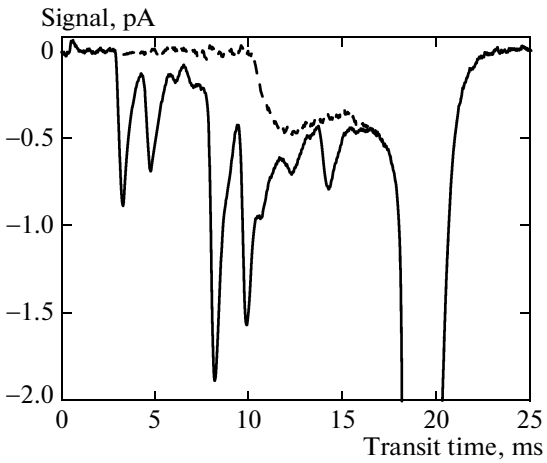

Fig. 1. Results from a time-of-flight mobility experiment performed at 0.991 K as reported in [22]. The solid curve shows the signal arriving at the collector as a function of time. The dashed curve is the signal after an algorithm has been used to remove the peaks. The length of the experimental cell is 6.15 cm and the drift field is 82.1 V cm^{-1}.

there are other negatively charged objects of unknown physical structure [14–21]. These have been called the "exotic ions" [15]. The solid curve in Fig. 1 shows data obtained in a recent time–of–flight mobility experiment at 0.991 K [22]. In this experiment, ions entered the liquid from a continuous electrical discharge in helium vapor above the surface of the liquid. The discharge was produced by a voltage applied between electrodes positioned in the vapor. After the ions entered the liquid, gate grids were used to allow a pulse of negative ions to enter the upper part of the experimental cell. These ions moved through the cell under the influence of a uniform drift field and the charge arriving at a collector at the bottom of the cell was recorded as a function of time. In Fig. 1, we can see a strong signal at a time of around 19 ms coming from the NEB. In addition, there is a series of peaks at earlier times coming from the exotic ions. Figure 1 clearly shows at least ten exotic ions; more recent experiments [23] have resolved 18 ions, each with a different mobility.

We can make a fit to each peak and then subtract the peak from the measured total signal. When this is done, a smoothly varying background signal is revealed as shown by the dashed curve in Fig. 1. The continuous background has a cutoff at a time that is approximately one half of the arrival time of the NEB. The time at which the cutoff appears in the signal is inversely proportional to the drift field, indicating that the background arises from ions. These ions must have a continuous distribution of mobility, and therefore presumably a continuous distribution of size.

It is interesting that although the signal from each individual exotic ion is much smaller than the signal from the NEB, the total signal from the exotic ions (including the continuous background) is of a magnitude comparable to the NEB signal (typically 20% to 50%).

At a critical velocity v_c, each of the exotic ions (except the fastest ion F) nucleates a vortex ring and becomes trapped on it [18]. The critical velocity is larger than the critical velocity for the NEB, indicating that the ions are smaller than the NEB. Since v_c increases progressively with an increase in ion mobility, each of the exotic ions appears to be singly charged.

A rough estimate of the ion size can be made from the measured mobility. Since the mean free path of a roton at temperatures around 1 K is large compared to the bubble size, the drag exerted on a moving bubble should be proportional to the cross-sectional area of the bubble. Hence, the mobility should vary approximately as the inverse square of the radius. Based on this, the radius of the fastest ion is found to be around 8 Å [17].

Presently, there is no accepted theory of the makeup of the exotic ions. Three ideas and their associated difficulties are as follows.

1—**Impurity model.** Impurity atoms that have acquired an extra electron could form bubbles with a size in the range of the exotic ions. However, an electron that is bound to an impurity with a high electron affinity (e.g., greater than 2 eV) would have a wave function that decreases very rapidly with distance. This would result in a snowball [24] or a bubble of a very small radius. Thus, in order for impurities to be the explanation of the exotic ions, the impurities have to have low electron affinity. It is also possible that there are impurities that do not form negative ions in the vacuum but which bind an electron in a bubble when in liquid helium. A serious difficulty with the impurity model is that the number of impurities that might be present in liquid helium is very small; it is difficult to believe that there can be 18 different impurities with the required electron affinity, and that the same impurities occur in different labs in different countries. Also, a theory based on impurities cannot explain the continuous background.

2—**Helium ion model.** Negative ions of a helium atom [25] or helium dimer [26] have been studied and their lifetime measured in a number of experiments. A negative ion immersed in liquid helium should form a bubble state if the binding of the electron to the atom (or dimer) is sufficiently weak. One problem is that the lifetimes of the known ions of helium atoms or dimers are much less than the time to traverse the mobility cells used in the experiments where exotic ions have been detected. Thus, the ions should decay before reaching the collector. In addition, the number of different ions is not sufficient to explain the observation of 18 distinct species of exotic ions. Also this model would not provide an explanation of the continuous background.

3—**Fission model** [27]. An electron entering the liquid has a complicated wave function. We can ask whether all of this wave function ends up in a single bubble. If the wave function ends up divided between two or more bubbles, it is not clear what would happen. One possibility is that the helium would make a measurement and determine that the electron is in one of the bubbles (call this bubble A). Then according to the Copenhagen interpretation of quantum mechanics, the wave function will suddenly change such that it is nonzero only in bubble A. The other bubbles, which contain no wave function, will collapse. But if this does not happen and the bubbles containing only a fraction of the wave function are stable, these should be smaller than the NEB and could provide an explanation of the exotic ions. Since the fraction of the wave function ending up in a bubble could have any value, this theory could explain the continuous distribution of mobility. In addition, it has been pointed out [27] that there is a mechanism that could lead to bubbles containing particular discrete fractions of the wave function, and this might explain the 18 ions with discrete values of mobility.

In this paper, we discuss how the possible experiments may allow distinguishing between these three models.

2. THEORETICAL MODEL

Shikin has written an excellent review of the properties of ions in liquid helium [24], and more recently there have been detailed calculations for ions of particular interest [28–33]. We first review a procedure for calculating the properties of a normal electron bubble. As already mentioned, the size of an NEB can be estimated from the expression for the energy given in Eq. (1). However, there are some limitations of this formula.

(a) The electron wave function penetrates into the bubble wall. This is neglected in the derivation of Eq. (1).

(b) In Eq. (1), the energy of the bubble surface is taken to be the surface area times the surface tension as measured in a macroscopic experiment. There should be corrections to the energy due to the curvature of the surface, and also because the interaction of the electron with the helium would modify the density profile of the surface.

(c) Equation (1) does not account for any variation of the surface energy per unit area with the pressure in the bulk liquid.

(d) The electric field of the electron polarizes the liquid surrounding the bubble and gives an inward force reducing the size of the bubble.

These effects can be taken into account by using a density functional for the helium. In previous work [6], we have used a simple density-functional model to calculate the properties of a normal electron bubble allowing for these effects. The Schrödinger equation for the electron was taken to be

$$-\frac{\hbar 2}{2m}\nabla^2\psi + V\psi = E_{\rm el}\psi, \tag{5}$$

where the potential $V(\mathbf{r})$ was given by $U_{\rm int}\rho(\mathbf{r})$, with $\rho(\mathbf{r})$ being the helium density at position $\mathbf{r}$. The coefficient $U_{\rm int}$ was set to have the value 1.1×10^{-11} cm^5 s^{-2}, such that the potential acting on the electron when it is in bulk helium at zero pressure is 1 eV. The free energy of the nonuniform liquid was taken to be [6]

$$\int[f(\rho) + \lambda|\nabla\rho|^2]dV, \tag{6}$$

where $f(\rho)$ is the free energy per unit volume of the liquid with a uniform density ρ, and the term $\lambda|\nabla\rho|^2$ is the extra energy per unit volume present when there is a gradient in density. The function $f(\rho)$ was determined by making a fit to the sound velocity at positive pressures; the details of this are given in the Appendix. The pressure is related to f by

$$P = -f + \rho\frac{\partial f}{\partial\rho}. \tag{7}$$

The plots of the variations of $f(\rho)$ and $P(\rho)$ with ρ are presented in Fig. 2.

It can be shown [6] that in this model, the density of the liquid satisfies the equation

$$\nabla^2\rho = \frac{1}{2\lambda}\left[\frac{\partial f}{\partial\rho} - \frac{\partial f}{\partial\rho}\bigg|_{\rho=\rho_1} + U_{\rm int}|\psi|^2\right], \tag{8}$$

where ρ_1 is the density of bulk liquid and λ is a parameter related to the surface tension (see the Appendix). Thus, to find the energy of the electron and the density distribution of the liquid around the bubble, we have to solve two coupled differential equations (Eqs. (5) and (8)) with appropriate boundary conditions. The solution of these equations is straightforward to find by numerical methods. This calculation has been improved in [34] through the use of a more sophisticated density functional scheme.[2] Once the density profile around the NEB was calculated, it was possible [34] to find the photon energies E_{1S-1P} and E_{1S-2P} required to excite the electron from the ground $1S$ state to the $1P$ and $2P$ states. These energies were calculated for liquid pressures up to the freezing pressure. The results were in excellent agreement with experiment [3–5]. More recent calculations suggest that there may also be a loosely bound $3P$ state [35].[3] However, the properties of this state are very sensitive to the exact height of the barrier provided by the helium, but this height has a substantial uncertainty [1]. In a subsequent paper, the same model was used to calculate the negative pressure P_c at which the NEB became unstable against explosion [36].

[2] Note that in these calculations, the effect of the polarization energy was not included.

[3] In addition, the matrix element to this state is very small.

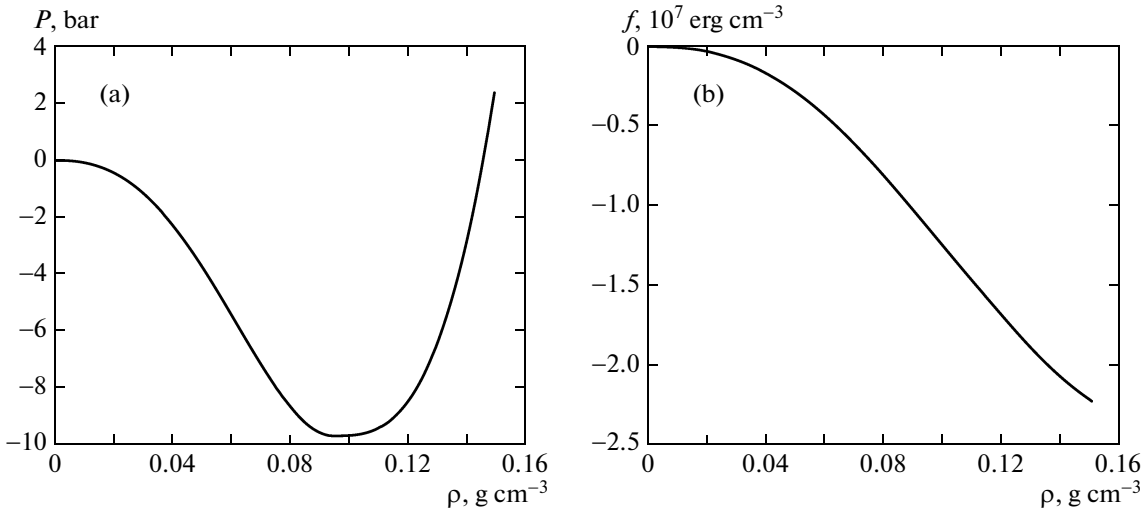

Fig. 2. (a) Pressure as a function of density, and (b) energy per unit volume as a function of density.

One would like to extend this type of calculation to find the size of a bubble containing a negative impurity ion. However, this appears to be difficult. Ideally, such a calculation needs to take account of (a) the Van der Waals attraction between the ion core and the liquid helium, (b) the polarization of the liquid due to the charge of the extra electron, (c) the interaction of the extra electron with the ion core, (d) the repulsive interaction between the electron with the surrounding helium, and (e) the surface energy of the helium. Using a density functional approach, it would be straightforward to include all of these effects except (c), the interaction of the extra electron with the ion core. One approach would be to model this interaction by means of some form of pseudo-potential and set the strength of this potential so as give the correct magnitude for the electron affinity, i.e., so as to give the correct binding of the "last electron" to the free atom. This would seem an appropriate approach because one expects that the electron with the weakest binding to the atom would generally have a wave function that extends out the furthest and is therefore most important in pushing the helium away and determining the radius of the bubble. However, this is complicated because for different atoms, the last electron can be in states of different angular momentum. For most atoms, the angular momentum is nonzero,[4] and hence the shape of the bubble in helium would be nonspherical.

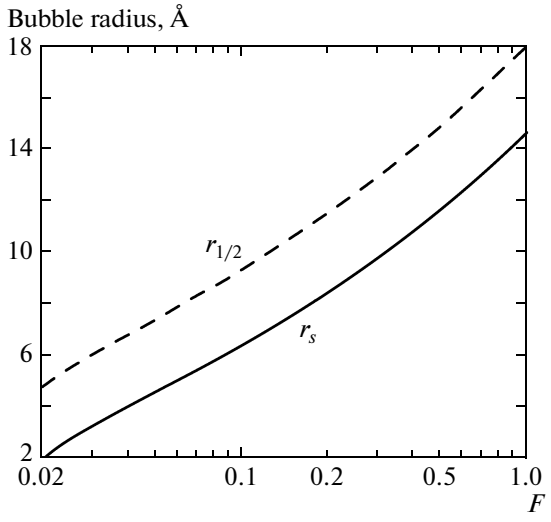

Fig. 3. Bubble radius on the fission model as a function of the fraction F defined in the text (r_s is the radius at which the helium density first becomes nonzero and $r_{1/2}$ is the radius at which the density equals half of the bulk density).

3. RESULTS AND DISCUSSION

For the reasons just discussed, we restrict attention to detailed calculations for the fission model.[5] We solve Eqs. (5) and (8) with ψ normalized such that the integral of $|\psi|^2$ takes a value F that is less than unity. Results for the bubble radius as a function of F are shown in Fig. 3; these results are for the electron in the lowest-energy $1S$ state. Examples of the density profile around the bubble and the electron wave function are shown in Fig. 4. We then calculate the energies of the $1P$ and $2P$ states using the helium density profile found for the $1S$ state.[6] The photon energies needed for excitation to the $1P$ and $2P$ states are plotted in Fig. 5 and

[4] For a review of negative ions, see [37].

[5] We do not include the effect of the polarization energy in these calculations since it is a small effect.

[6] The calculation of E_{1S-1P} and E_{1S-2P} is based on the Franck-Condon principle.

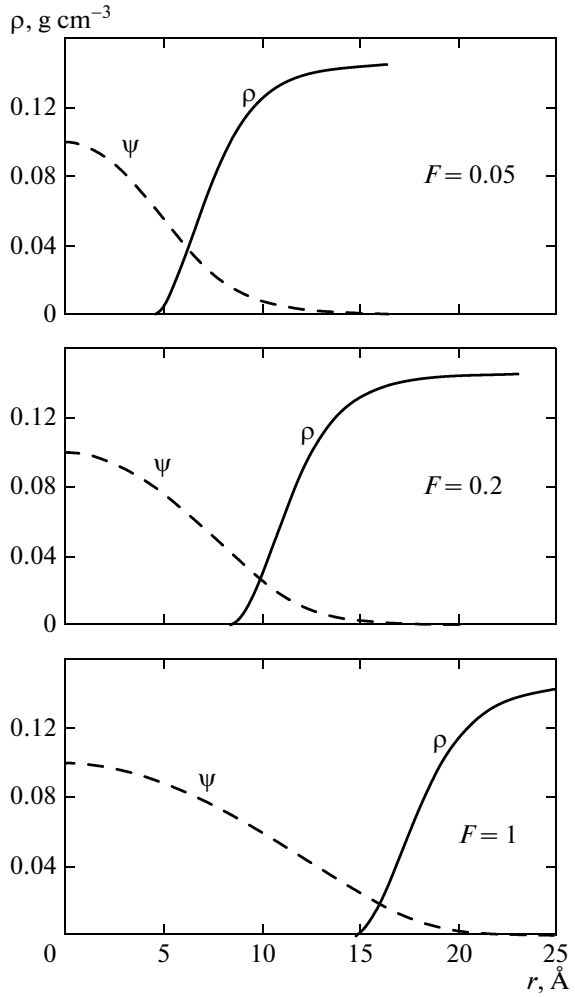

Fig. 4. Helium density profile $\rho(r)$ and the electron wave function $\psi(r)$ for different values of the fraction F discussed in the text. In each part of the figure, the wave function ψ has been scaled to have the value 0.1 at the origin.

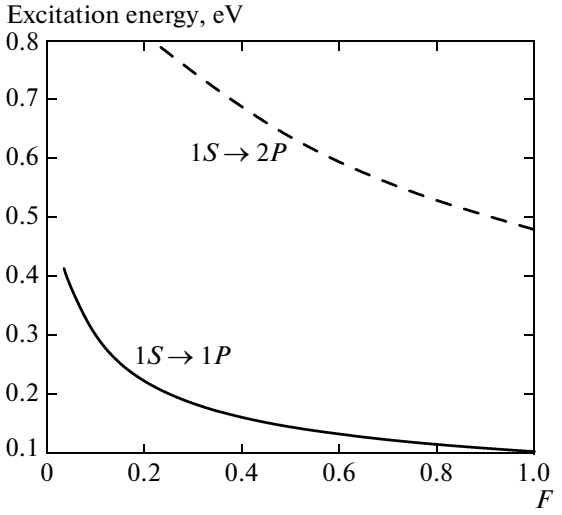

Fig. 5. Photon energies for the $1S$ to $1P$ and $1S$ to $2P$ transitions according to the fission model as a function of the fraction F defined in the text. The curve for the $1S$ to $2P$ transition terminates when the $2P$ state ceases to be bound in the bubble.

the dependence of the critical explosion pressure on F is shown in Fig. 6.

We now want to discuss how comparisons of the results of the calculations in this paper with experiment may be used to test the different possible theories of the exotic ions.

We first note that the mobility measurements are of limited use in testing the theories. For each exotic ion, one can use the mobility to estimate the radius. As a first approximation, it is expected that the mobility of an ion should be inversely proportional to the square of the radius. Thus, for a particular exotic ion with mobility μ_i, one can estimate the radius as

$$R_i = R_{NEB}\sqrt{\frac{\mu_{NEB}}{\mu_i}}, \qquad (9)$$

where μ_{NEB} and R_{NEB} are the mobility and the radius of the NEB. At first sight, it might appear possible to compare this radius with the results presented in Fig. 3. However, the accuracy of formula (9) is unknown. For example, Eq. (9) takes no account of the effective mass of the ion, while it is well known that the mobility of an ion moving through a gas of atoms depends on the mass of the ion (see, for example, [38]). For positive impurity ions in helium, the effect of a mass variation has been explicitly demonstrated in [39] by means of experiments with different isotopes of calcium. Even if a radius could be estimated from Eq. (9), it would not be clear how to relate this to the theoretical calculations made in this paper. Should this radius be compared with the calculated r_s, or with $r_{1/2}$, or something else? As far as we can see, the most important results coming from the mobility experiments are that there are at least 18 ions with different mobility and that there are, in addition, ions with a continuous distribution of mobility.

Measurements of the optical absorption would provide the following information.

1. For the fission model, a measurement of either E_{1S-1P} or E_{1S-2P} would determine the value of the fraction F. The calculations presented here would then give a definite prediction for the other energy and would provide a test of the theory.

2. In the fission model, the bubble is spherical. For a spherical bubble, the transitions are limited to $\Delta l = \pm 1$ and the matrix element for a transition to the $3P$ state (if it is indeed a bound state) is very small. Hence, there should be only two photon energies that can be absorbed, and if more than two photon energies are found, this indicates that the fission model must be incorrect.

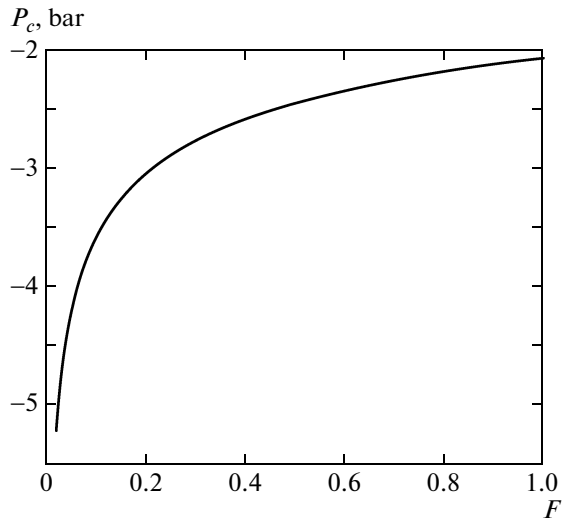

Fig. 6. Critical pressure P_c at which a bubble explodes as a function of the fraction F defined in the text.

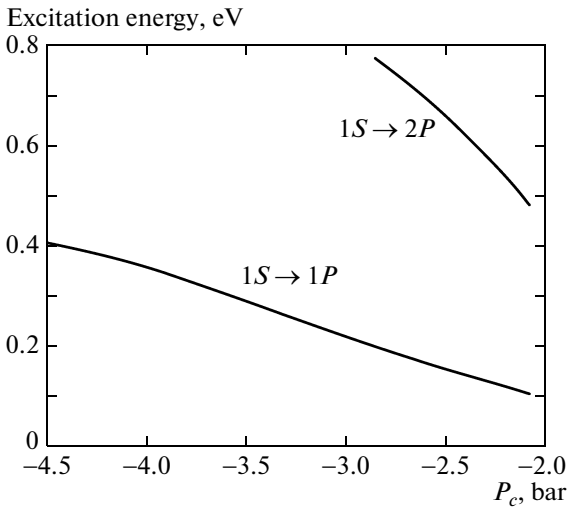

Fig. 7. The variation of the excitation energies E_{1S-1P} and E_{1S-2P} as a function of the critical explosion pressure P_c as found from the fission model.

Measurements of the explosion pressure could be used to determine the fraction F in the fission model. Using the results of measurements of P_c in conjunction with optical measurements would provide much more stringent tests. In Fig. 7, we show how the excitation energies E_{1S-1P} and E_{1S-2P} are predicted to vary with the explosion pressure P_c based on the fission model.

It is a great pleasure to contribute this article to the Festschrift for Alexander Andreev, and we wish him many more years of happy science. We thank M. Barranco, L. N. Cooper, and G. M. Seidel for helpful discussions. This work was supported in part by the United States National Science Foundation under Grant No. DMR 0965728.

APPENDIX

The free energy function $f(\rho)$ was estimated by the method described in [40]. The estimate used the results for the pressure dependence of the sound velocity as measured in [41]. We have applied a small correction to the formulas for $f(\rho)$ given in [40] because in that paper the pressure was incorrectly taken to be in bars whereas in [41], in fact, atmospheres were used as the unit of pressure [42]. With this change, we find

$$f(\rho) = f_c + (\rho - \rho_c)f_1 + (\rho - \rho_c)^3 f_3 + (\rho - \rho_c)^4 f_4, \quad \rho < \rho_c,$$
$$f(\rho) = \frac{b^2}{9}\left(\frac{\rho^3}{6} - \rho_c\rho^2 + \rho_c^2\rho\log\rho + s\rho + \frac{\rho_c^3}{3} - \frac{9P_c}{b^2}\right), \quad \rho > \rho_c, \tag{A.1}$$

where, in cgs units,

$$\begin{aligned} \rho_c &= 0.0941561, \quad P_c = -9.64803 \times 10^6, \\ b &= 1.40243 \times 10^6, \quad s = 2.43656 \times 10^{-2}, \\ f_c &= -1.12213 \times 10^7, \quad f_1 = -2.21646 \times 10^8, \\ f_3 &= 2.12317 \times 10^{10}, \quad f_4 = 1.02739 \times 10^{11}. \end{aligned} \tag{A.2}$$

The parameter λ is related to the surface tension by the formula

$$\alpha = 2\int_0^{\rho_0} \sqrt{\lambda[f(\rho) - (\rho/\rho_0)f(\rho_0)]}\,d\rho, \tag{A.3}$$

where ρ_0 is the density of the liquid at zero pressure. This relation can be used to set the value of λ. At the time of publication of [40], the accepted value [43] of α was 0.355 erg cm^{-2}, which gave the result $\lambda = 6.8 \times 10^{-7}$ g^{-1} cm^7 s^{-2}. Since then, the accepted value has changed [27] to 0.375 erg cm^{-2}, which leads to the value $\lambda = 7.5516 \times 10^{-7}$ g^{-1} cm^7 s^{-2}.

REFERENCES

1. M. A. Woolf and G. W. Rayfield, Phys. Rev. Lett. **15**, 235 (1965); W. T. Sommer, Phys. Rev. Lett. **12**, 271 (1964).
2. P. Roche, G. Deville, N. J. Appleyard, and F. I. B. Williams, J. Low Temp. Phys. **106**, 565 (1997).
3. C. C. Grimes and G. Adams, Phys. Rev. B: Condens. Matter **41**, 6366 (1990).
4. C. C. Grimes and G. Adams, Phys. Rev. B: Condens. Matter **45**, 2305 (1992).
5. A. Y. Parshin and S. V. Pereverzev, JETP Lett. **52** (5), 282 (1990); A. Y. Parshin and S. V. Pereverzev, Sov. Phys. JETP **74** (1), 68 (1992); S. Pereversev and A. Y. Parshin, Physica B (Amsterdam) **197**, 347 (1994).

6. J. Classen, C.-K. Su, M. Mohazzab, and H. J. Maris, Phys. Rev. B: Condens. Matter **57**, 3000 (1998).
7. V. A. Akulichev and Y. Y. Boguslavskii, Sov. Phys. JETP **35**, 1012 (1972).
8. L. Meyer and F. Reif, Phys. Rev. **110**, 279 (1958); L. Meyer and F. Reif, Phys. Rev. Lett. **5**, 1 (1960).
9. F. Reif and L. Meyer, Phys. Rev. **119**, 1164 (1960).
10. K. W. Schwarz, Phys. Rev. A: At., Mol., Opt. Phys. **6**, 837 (1972).
11. G. W. Rayfield and F. Reif, Phys. Rev. [Sect.] A **136**, A1194 (1964).
12. J. Poitrenaud and F. I. B. Williams, Phys. Rev. Lett. **29**, 1230 (1972); J. Poitrenaud and F. I. B. Williams, Phys. Rev. Lett. **32**, 1213 (1974).
13. T. Ellis and P. V. E. McClintock, Phys. Rev. Lett. **48**, 1834 (1982); T. Ellis and P. V. E. McClintock, J. Phys. C: Solid State Phys. **16**, L485 (1983).
14. C. S. M. Doake and P. W. F. Gribbon, Phys. Lett. A **30**, 251 (1969).
15. G. G. Ihas and T. M. Sanders, Phys. Rev. Lett. **27**, 383 (1971).
16. G. G. Ihas and T. M. Sanders, in *Proceedings of the 13th International Conference on Low Temperature Physics (LT-13), Boulder, Colorado, United States, August 21–25, 1972*, Ed. by K. D. Timmerhaus, W. J. O'Sullivan, and E. F. Hammel (Plenum, New York, 1974), Vol. 1, p. 477.
17. G. G. Ihas, PhD Thesis (University of Michigan, Ann Arbor, Michigan, United States, 1971).
18. V. L. Eden and P. V. E. McClintock, Phys. Lett. A **102**, 197 (1984).
19. V. L. Eden and P. V. E. McClintock, in *Proceedings of the 75th Jubilee Conference on Liquid ^{4}Helium*, Ed. by J. G. M. Armitage (World Scientific, Singapore, 1983), p. 194.
20. V. L. Eden, MPhil Thesis (University of Lancaster, Lancaster, United Kingdom, 1986).
21. C. D. H. Williams, P. C. Hendry, and P. V. E. McClintock, Jpn. J. Appl. Phys. **26** (Suppl. 26–3), 105 (1987).
22. W. Wei, Z. Xie, G. M. Seidel, and H. J. Maris, J. Low Temp. Phys. **171**, 178 (2013).
23. W. Wei, Z. Xie, G. M. Seidel, and H. J. Maris, J. Low Temp. Phys. (2015) (in press).
24. V. B. Shikin, Sov. Phys.—Usp. **20**, 226 (1977).
25. B. Brehm, M. A. Gusinow, and J. L. Hall, Phys. Rev. Lett. **19**, 737 (1967); P. Kristensen, U. V. Pedersen, V. V. Petrunin, T. Andersen, and K. T. Chung, Phys. Rev. A: At., Mol., Opt. Phys. **55**, 978 (1997); D. L. Mader and R. Novick, Phys. Rev. Lett. **29**, 199 (1972); L. M. Blau, R. Novick, and D. Weinflash, Phys. Rev. Lett. **24**, 1268 (1970).
26. Y. K. Bae, M. J. Coggiola, and J. R. Peterson, Phys. Rev. Lett. **52**, 747 (1984); T. J. Kvale, R. N. Compton, G. D. Alton, J. S. Thompson, and D. J. Pegg, Phys. Rev. Lett. **56**, 592 (1986); T. Andersen, L. H. Andersen, N. Bjerre, P. Hvelpund, and J. H. Posthumus, J. Phys. B: At., Mol. Opt. Phys. **27**, 1135 (1994).
27. H. J. Maris, J. Low Temp. Phys. **120**, 173 (2000).
28. P. D. Grigor'ev and A. M. Dygaev, J. Exp. Theor. Phys. **88** (2), 325 (1999).
29. W. F. Schmidt, K. F. Volykhin, A. G. Khrapak, and E. Illenberger, J. Electrost. **47**, 83 (1999).
30. A. G. Khrapak, JETP Lett. **86** (4), 252 (2007).
31. A. G. Khrapak and W. F. Schmidt, Int. J. Mass Spectrosc. **277**, 236 (2008).
32. F. Ancilotto, M. Barranco, and M. Pi, Phys. Rev. B: Condens. Matter **80**, 174504 (2009).
33. A. G. Khrapak and W. F. Schmidt, Low Temp. Phys. **37** (5), 387 (2011).
34. V. Grau, M. Barranco, R. Mayol, and M. Pi, Phys. Rev. B: Condens. Matter **73**, 064502 (2006); M. Pi, M. Barranco, V. Grau, and R. Mayol, Int. J. Mod. Phys. B **20**, 5291 (2006).
35. J. Barragan, D. Mateo, M. Pi, F. Salvat, M. Barranco, and H. J. Maris, J. Low Temp. Phys. **171**, 171 (2013).
36. M. Pi, M. Barranco, R. Mayol, and V. Grau, J. Low Temp. Phys. **139**, 397 (2005); M. Pi, M. Barranco, and R. Mayol, J. Low Temp. Phys. **138**, 463 (2005).
37. T. Andersen, Phys. Rep. **394**, 157 (2004).
38. E. W. McDaniel and E. A. Mason, *Transport Properties of Ions in Gases* (Wiley, New York, 1988).
39. W. I. Glaberson and W. W. Johnson, J. Low Temp. Phys. **20**, 313 (1975).
40. H. J. Maris, J. Low Temp. Phys. **94**, 125 (1994).
41. B. M. Abraham, Y. Eckstein, J. B. Ketterson, M. Kuchnir, and P. R. Roach, Phys. Rev. A: At., Mol., Opt. Phys. **1**, 250 (1970).
42. F. Caupin and S. Balibar, Phys. Rev. B: Condens. Matter **64**, 064507 (2001).
43. M. Iino, M. Suzuki, and A. Ikushima, J. Low Temp. Phys. **61**, 155 (1985).